SANDIA REPORT
SAND 2009-8295
Unlimited Release
December 2009

Aft-Body Loading Function for Penetrators Based on the Spherical Cavity-Expansion Approximation

Donald B. Longcope, Thomas L. Warren, and Henry Duong

Prepared by
Sandia National Laboratories
Albuquerque, New Mexico 87185 and Livermore, California 94550

Sandia is a multiprogram laboratory operated by Sandia Corporation,
a Lockheed Martin Company, for the United States Department of Energy's
National Nuclear Security Administration under Contract DE-AC04-94AL85000.

Approved for public release; further dissemination unlimited.

Sandia National Laboratories

Issued by Sandia National Laboratories, operated for the United States Department of Energy by Sandia Corporation.

NOTICE: This report was prepared as an account of work sponsored by an agency of the United States Government. Neither the United States Government, nor any agency thereof, nor any of their employees, nor any of their contractors, subcontractors, or their employees, make any warranty, express or implied, or assume any legal liability or responsibility for the accuracy, completeness, or usefulness of any information, apparatus, product, or process disclosed, or represent that its use would not infringe privately owned rights. Reference herein to any specific commercial product, process, or service by trade name, trademark, manufacturer, or otherwise, does not necessarily constitute or imply its endorsement, recommendation, or favoring by the United States Government, any agency thereof, or any of their contractors or subcontractors. The views and opinions expressed herein do not necessarily state or reflect those of the United States Government, any agency thereof, or any of their contractors.

Printed in the United States of America. This report has been reproduced directly from the best available copy.

Available to DOE and DOE contractors from
U.S. Department of Energy
Office of Scientific and Technical Information
P.O. Box 62
Oak Ridge, TN 37831

Telephone: (865) 576-8401
Facsimile: (865) 576-5728
E-Mail: reports@adonis.osti.gov
Online ordering: http://www.osti.gov/bridge

Available to the public from
U.S. Department of Commerce
National Technical Information Service
5285 Port Royal Rd.
Springfield, VA 22161

Telephone: (800) 553-6847
Facsimile: (703) 605-6900
E-Mail: orders@ntis.fedworld.gov
Online order: http://www.ntis.gov/help/ordermethods.asp?loc=7-4-0#online

SAND 2009-8295
Unlimited Release
December 2009

Aft-Body Loading Function for Penetrators Based on the Spherical Cavity-Expansion Approximation

Donald B. Longcope, Computational Structural Mechanics and Applications Department
Thomas L. Warren, former Sandian, and
Henry Duong, Weapon Safety Basis Engineering Department
Sandia National Laboratories
P.O. Box 5800
Albuquerque, New Mexico 87185-MS0836

Abstract

In this paper we develop an aft-body loading function for penetration simulations that is based on the spherical cavity-expansion approximation. This loading function assumes that there is a pre-existing cavity of radius a_o before the expansion occurs. This causes the radial stress on the cavity surface to be less than what is obtained if the cavity is opened from a zero initial radius. This in turn causes less resistance on the aft body as it penetrates the target which allows for greater rotation of the penetrator. Results from simulations are compared with experimental results for oblique penetration into a concrete target with an unconfined compressive strength of 23 MPa.

ACKNOWLEDGMENTS

The authors wish to thank M. J. Forrestal for helping us evaluate the limit of the present solution as the cavity radius approaches infinity.

CONTENTS

Introduction 6
Analytical Model 7
Results 11
Conclusions 18
References 19
Distribution 21

FIGURES

Figure 1. Schematic of the Projectile with its Dimensions in mm 11
Figure 2. a/a_o vs. b/a for Expansion Velocities Between 0 and 700 m/s 12
Figure 3. $\sigma_r(a)/Y$ vs. a/a_o for Expansion Velocities Between 0 and 700 m/s 13
Figure 4. Cut Away View of the Finite Element Mesh 14
Figure 5. Detail of $\sigma_r(a)/Y$ *vs.* a/a_0 for expansion velocities Between 0 and 200 m/s 15
Figure 6. Radial Stress vs. Expansion Velocity for the Three Cavity Expansion Models ... 16

TABLES

Table 1. Material Properties for 23 MPa Concrete 12
Table 2. Material Constants for the Projectile 14
Table 3. Cavity Expansion Coefficients and Free Surface Effect Constants 16
Table 4. Projectile Rest Angles 17

Introduction

Computational modeling of penetration and perforation remains an active field of esearch. A literature search on this topic reveals numerous recent publications that propose new methods or improve existing ones. There has been considerable effort and progress in the development of various codes (based on different representations of the conservation laws for a continuum: Lagrangian, Eulerian, Arbitrary Lagrangian-Eulerian, etc.) that serve as powerful and versatile computational tools which are used to solve complex problems. However, at present, the time required to complete a single penetration run is still excessive and prohibits any prospect for streamlining the penetration analysis for use as an overall design tool that would permit numerous simulations.

In cases where the deformation of the target can be captured by a known analytical model and where the primary interest is in the structural response of the projectile, the penetration analysis can then be reduced to modeling the projectile by itself. The target is replaced by a known forcing function that approximates its resistance. This eliminates the need to model the target and furthermore eliminates the need for a contact algorithm, which leads to substantial savings in execution time.

For the penetration of targets that have an angle of obliquity and/or angle of attack there is an unsymmetric loading that acts on both the nose and shank of the projectile. To account for the loading on the shank, we have developed a new model which applies a load on the shank of the projectile that is less than that which acts on the nose of the projectile. Models have been developed by Longcope et al. [1] and Warren and Poormon [2] that consider a cavity in a finite domain of target material to model free surface effects. In this present work we consider a spherical cavity that is expanded from a non-zero initial radius equal to the radius of the shank of the projectile. The motivation for this approach is that frequently in penetration events, a tunnel is created over most of the trajectory and its cross-section is approximately that of the aft-body. We envision that the nose creates the tunnel and the aft-body elongates the cross-section a small amount. The velocity dependent radial stress at the cavity surface of the target material is then applied to the shank of the projectile producing less resistance than that of a cavity being opened up from a zero initial radius. This new model will then be employed with the PRESTO/CE

methodology [3]. Results from the computer simulations are compared with experimental data for projectiles striking 23 MPa concrete targets at oblique angles [4].

Analytical Model

Analytical methods for penetration mechanics began with the work of Bishop, Hill, and Mott [5]. They developed equations for the quasi-static expansions of cylindrical and spherical cavities and used these equations to estimate forces on conical nose punches pushed slowly into metal targets. Goodier [6] developed a model to predict the penetration depth of rigid spheres launched into metal targets. His penetration model included target inertial effects, and he approximated the target response by results from the dynamic, spherically symmetric, cavity-expansion equations for an incompressible target material derived by Hill [7] and discussed by Hill [8] and Hopkins [9]. In more recent work [10-14] it has been shown that the radial stress at the cavity surface obtained from spherical cavity-expansion models can be accurately represented by a function of the form

$$\sigma_r(a) = c_1 + c_2 V_n + c_3 V_n^2 \quad , \tag{1}$$

where V_n is the target particle velocity at the cavity-target interface, a is the cavity radius, and $c_1, c_2,$ and c_3 are the cavity expansion fitting coefficients. The expression given in (1) is also consistent with the semi-empirical model developed by Forrestal et al. [15] for penetration into concrete targets.

The present analysis considers the dynamic, spherically symmetric expansion of an initial spherical cavity. Additionally, we assume that the material is incompressible which allows a closed-form representation of the response. Then the equations of momentum and mass conservation are

$$\frac{\partial \sigma_r}{\partial r} + \frac{2(\sigma_r - \sigma_\theta)}{r} = -\rho\left(\frac{\partial \upsilon}{\partial t} + \upsilon \frac{\partial \upsilon}{\partial r}\right) \tag{2a}$$

$$\frac{\partial \upsilon}{\partial r} + \frac{2\upsilon}{r} = 0 \quad , \tag{2b}$$

where σ_r, σ_θ are the radial and hoop components of the Cauchy stress, measured positive in compression, and ρ is the constant density of the material. Particle displacement u and particle velocity υ in the radial direction (outward motion taken positive) are related by

$$\frac{\partial u}{\partial t} = \upsilon\left(1 - \frac{\partial u}{\partial r}\right) \quad . \tag{3}$$

The assumption of incompressibility allows the equation for conservation of mass given by (2b) to be directly integrated to give

$$\upsilon = \frac{a^2 \dot{a}}{r^2} \quad , \tag{4}$$

where a and $\dot{a}$ are the radius and expansion velocity of the spherical cavity. We first consider the elastic response. Using (4) with the small amplitude approximation $\upsilon = \partial u / \partial t$ gives the displacement as

$$u = \frac{a^3 - a_o^3}{3r^2} \quad , \tag{5}$$

where a_0 is the initial cavity radius. The small elastic strains are

$$\varepsilon_r = \frac{2\left(a^3 - a_o^3\right)}{3r^3} \tag{6a}$$

$$\varepsilon_\theta = -\frac{\left(a^3 - a_o^3\right)}{3r^3} \quad , \tag{6b}$$

where the strains are positive in compression. Using Hooke's law with Poisson's ratio equal to 1/2 and (6) gives

$$\sigma_r - \sigma_\theta = \frac{2E\left(a^3 - a_o^3\right)}{3r^3} \quad , \tag{7}$$

where E is Young's modulus. Conservation of momentum becomes

$$\frac{\partial \sigma_r}{\partial r} + \frac{4E\left(a^3 - a_o^3\right)}{3r^4} = -\rho\left[\frac{2a\dot{a}^2 + a^2\ddot{a}}{r^2} - \frac{2a^4\dot{a}^2}{r^5}\right] , \tag{8}$$

where the convective term in the equation of momentum conservation has been retained. Integrating (8) and assuming a constant expansion velocity (as in Forrestal et al. [12] where the $a\ddot{a}$ has a negligible effect in the equation for the depth of penetration) gives

$$\sigma_r = \frac{4E\left(a^3 - a_o^3\right)}{9r^3} + \rho\left[\frac{2a\dot{a}^2}{r} - \frac{a^4\dot{a}^2}{2r^4}\right] + f(t), \tag{9}$$

where $f(t)$ is an arbitrary function of time. If the radial stress is taken to vanish at infinity, then $f(t) \equiv 0$. It follows that the elastic radial stress at the cavity surface is

$$\sigma_r(a) = \frac{4}{9}E\left(1 - \frac{a_o^3}{a^3}\right) + \frac{3}{2}\rho\dot{a}^2 \quad . \tag{10}$$

As the radial deformation increases plastic deformation occurs. The material in the plastic region, $a \le r \le b$, is described by an incompressible Mohr-Coulomb yield criterion as discussed in Forrestal and Longcope [16] and Forrestal and Tzou [13]. Thus,

$$p = \left(\sigma_r + \sigma_\theta + \sigma_\phi\right)/3; \quad \sigma_\theta = \sigma_\phi \tag{11a}$$

$$\sigma_r - \sigma_\theta = \lambda p + \tau; \quad \tau = \left[(3-\lambda)/3\right]Y , \tag{11b}$$

where p is the pressure, λ and τ define the pressure-dependent shear strength, and Y is the uniaxial compressive strength. By rearranging (11), it follows that

$$2\left(\sigma_r - \sigma_\theta\right) = \alpha\left(\tau + \lambda\sigma_r\right), \tag{12}$$

where $\alpha = 6/(3 + 2\lambda)$. For plastic deformation the equation for conservation of momentum becomes

$$\frac{\partial \sigma_r}{\partial r} + \frac{\alpha\lambda\sigma_r}{r} = -\rho\left[\frac{2a\dot{a}^2 + \ddot{a}a^2}{r^2} - \frac{2a^4\dot{a}^2}{r^5}\right] - \frac{\alpha\tau}{r} \ . \tag{13}$$

Integrating (13) for a constant expansion velocity using the integrating factor $\Lambda = r^{\alpha\lambda}$ gives

$$\sigma_r = -\frac{2\rho a\dot{a}^2}{(\alpha\lambda - 1)r} + \frac{2\rho a^4\dot{a}^2}{(\alpha\lambda - 4)r^4} - \frac{\tau}{\lambda} + B(t)r^{-\alpha\lambda}, \tag{14}$$

where $B(t)$ is an arbitrary function of time to be determined from the conditions at the elastic-plastic interface.

We now use the interface conditions at $r=b$ to complete the solution. At the elastic-plastic interface the radial stress is continuous; therefore, equating (9) with $f(t) = 0$ and (14) at b gives

$$B(t) = b^{\alpha\lambda}\left\{\frac{2\rho\dot{a}^2}{\alpha\lambda - 1}\left(\frac{a}{b}\right) - \frac{2\rho\dot{a}^2}{\alpha\lambda - 4}\left(\frac{a}{b}\right)^4 + \frac{\tau}{\lambda} + \frac{4E}{9}\frac{\left(a^3 - a_o^3\right)}{b^3} + 2\rho\dot{a}^2\left(\frac{a}{b}\right) - \frac{\dot{a}^2}{2}\left(\frac{a}{b}\right)^4\right\}. \tag{15}$$

The radial stress at the cavity surface is

$$\sigma_r(a) = \left\{\frac{2\rho\dot{a}^2}{\alpha\lambda - 4} - \frac{2\rho\dot{a}^2}{\alpha\lambda - 1} - \frac{\tau}{\lambda} + \left(\frac{b}{a}\right)^{\alpha\lambda}\left[\frac{2\rho\dot{a}^2}{\alpha\lambda - 1}\left(\frac{a}{b}\right) - \frac{2\rho\dot{a}^2}{\alpha\lambda - 4}\left(\frac{a}{b}\right)^4\right.\right.$$
$$\left.\left. + \frac{\tau}{\lambda} + \frac{4E}{9}\frac{\left(a^3 - a_o^3\right)}{b^3} + 2\rho\dot{a}^2\left(\frac{a}{b}\right) - \frac{\dot{a}^2}{2}\left(\frac{a}{b}\right)^4\right]\right\}. \tag{16}$$

Next, we need an expression for a/b. As opposed to assuming the pressure is equal to zero in the elastic region as done by Forrestal and Tzou [13] and Warren et al. [17] we obtain an expression by using the Mohr-Coulomb expression (11) with Hooke's law (7) and equation (9) evaluated at the elastic-plastic interface b which gives

$$\tau\left(\frac{b}{a}\right)^4 + \rho\lambda\dot{a}^2\left[2\left(\frac{b}{a}\right)^3 - \frac{1}{2}\right] - \frac{2E}{3}\left(1 - \frac{a_o^3}{a^3}\right)\left(\frac{b}{a}\right) = 0. \tag{17}$$

This result indicates that a/b is a function of expansion velocity $\dot{a}$ and initial radius a_o.

Results

Experiments were conducted using an 83-mm-diameter, smooth-bore powder gun that launched 13 kg, 3 CRH ogive-nose, 4340 R_c 43 steel projectiles to striking velocities between 285 and 376 m/s into 23 MPa concrete targets that were angled at 15 and 30 degrees. The projectiles were fitted with sabots and obturators that separated from the projectiles before impact. Photographs from a high-speed, digital framing camera (Imacon Model 486) showed that the launch packages were stripped from the projectiles before impact. Digital photographs were also used to measure pitch and yaw angles. A Hall Intervelometer System measured striking velocities. Additionally, the projectiles also carried a Minpen data recorder that measured axial and lateral accelerations. Projectile rest angles were measured in the same plane as the orientation of the concrete impact surfaces whose normals were angled at 15 and 30 degrees to the striking velocities. A schematic of the projectile is shown in Fig. 1.

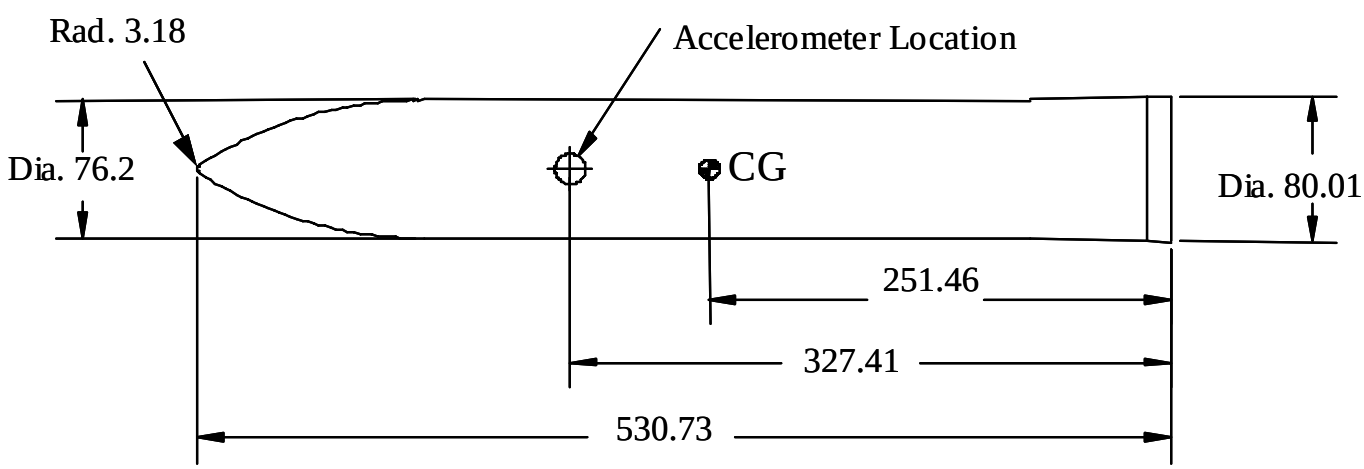

Figure 1. Schematic of the Projectile with its Dimensions in mm.

We consider the expansion of a spherical cavity in incompressible 23 MPa concrete. The parameters for this material [4] are given in Table 1. The first step in evaluating the radial stress at the cavity surface is to solve (17). We do this for a particular value of $\dot{a}$ by assuming a range of values of a/b and solving for a/a_o as shown in Fig. 2. For a given $\dot{a}$ we use the values of a/b

Table 1. Material Properties for 23 MPa Concrete

λ	τ (MPa)	Y (MPa)	E (GPa)	ρ (kg/m^3)
1.17	14.2	23.2	3.98	1910

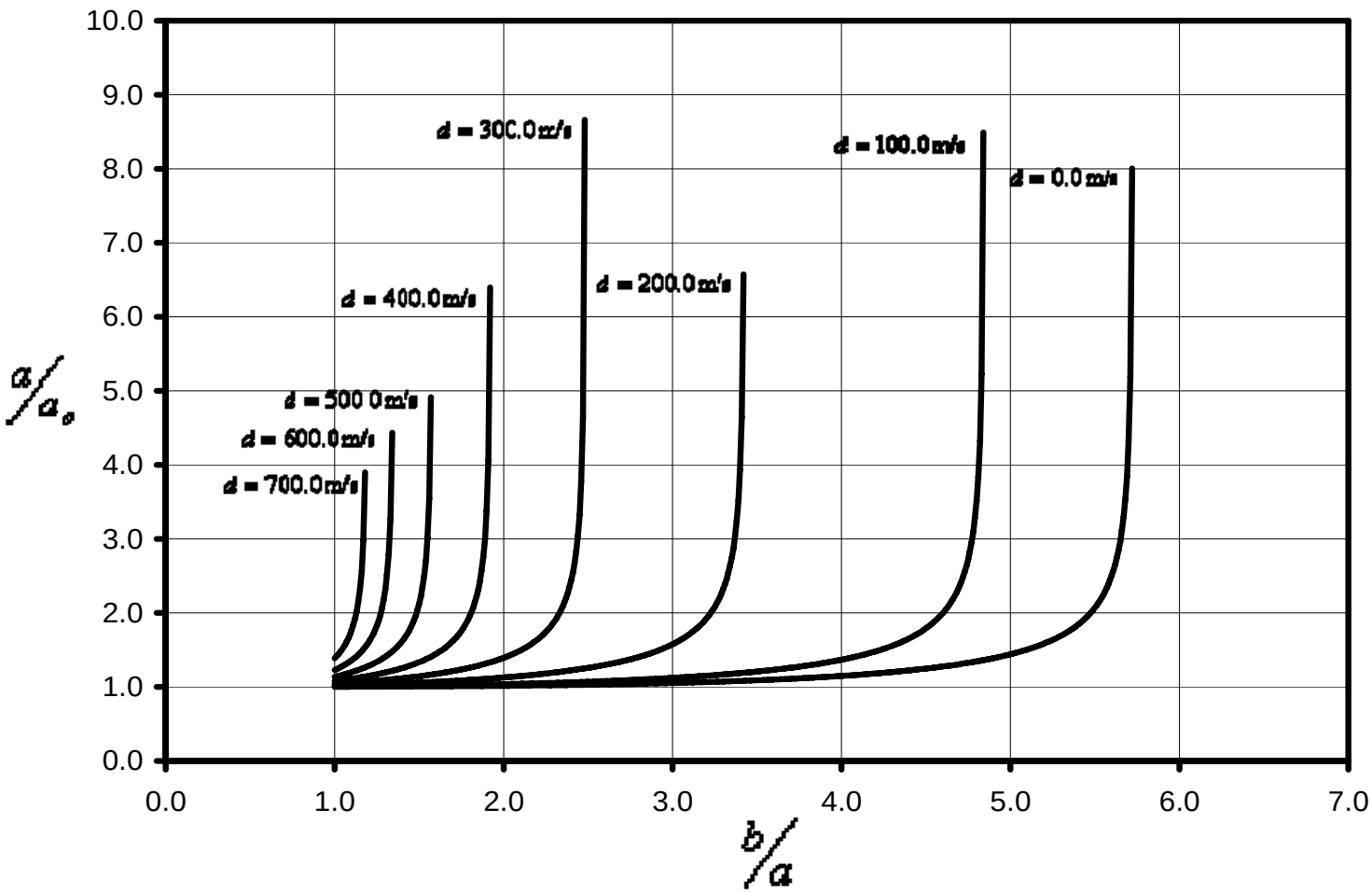

Figure 2. a/a_o vs. b/a **for Expansion Velocities between 0 and 700 m/s**

and a/a_o in (16) to obtain the radial stress at the cavity surface as shown in Fig. 3. It is observed that as a/a_o increases the value of the radial stress at the cavity surface becomes constant. The constant values of radial stress, obtained in the limit as a/a_0 approaches infinity, agree with the results of Forrestal and Tzou [13] when we set $\lambda = 0$ and neglect the convective derivative in the momentum equation in the elastic region.

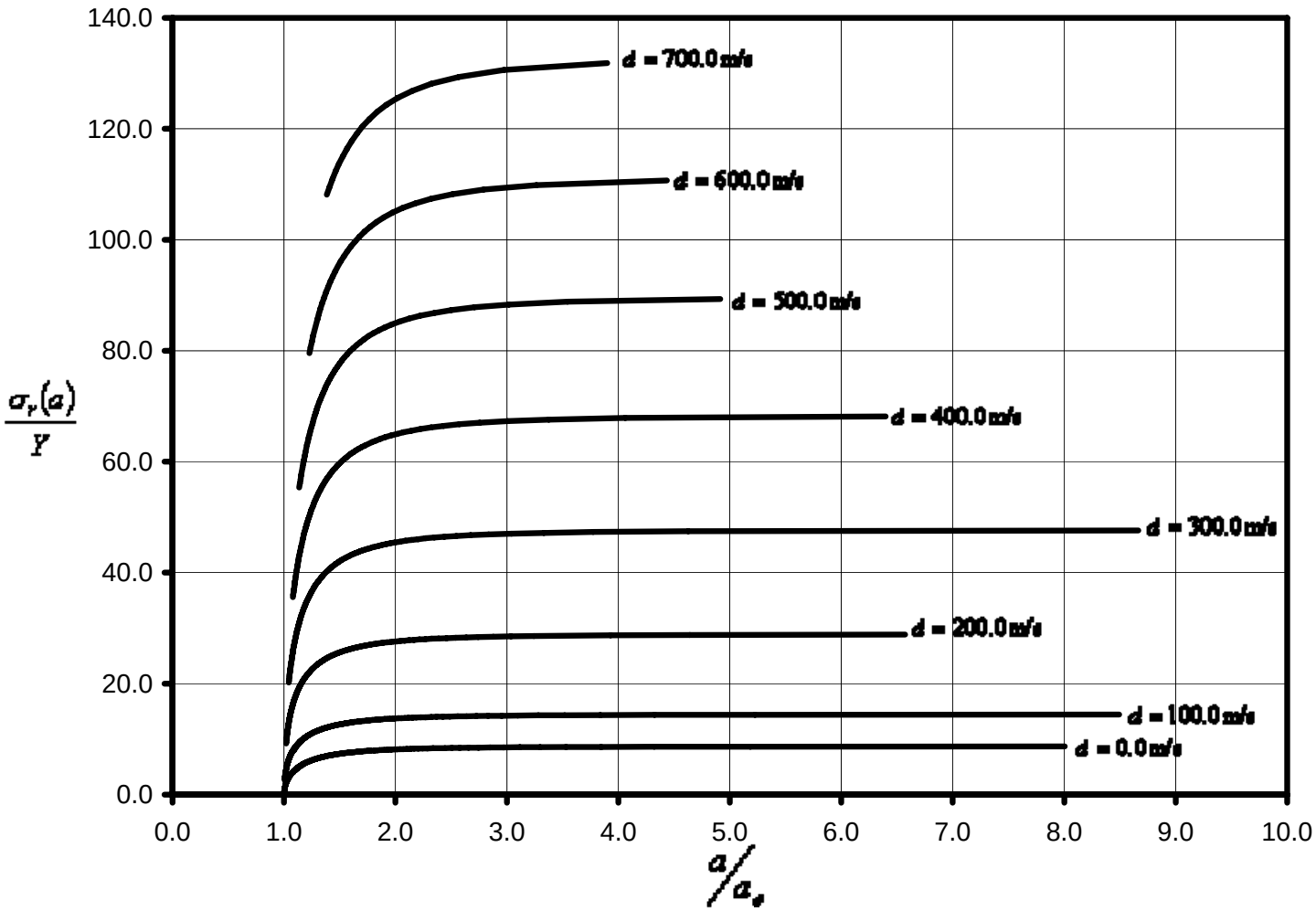

Figure 3. $\sigma_r(a)/Y$ vs. a/a_o **for Expansion Velocities Between 0 and 700 m/s**

We modeled the penetration experiments with the finite element code PRESTO [3] using the spherical cavity-expansion option. The penetrator mesh had 45294 constant strain hexahedral elements with 52776 nodes, and a cut away view of the mesh is shown in Fig. 4.

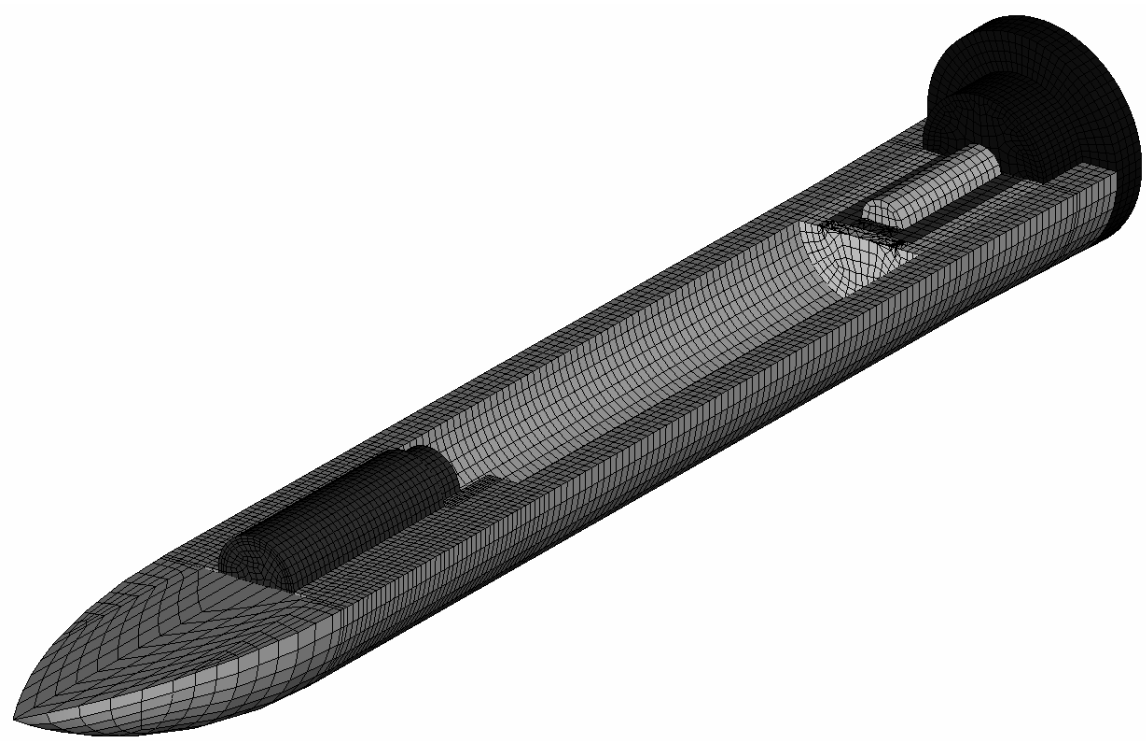

Figure 4. Cut Away View of the Finite Element Mesh

The penetrator case and all of its components were modeled using an elastic-plastic linear hardening constitutive model. The values of the material constants for this constitutive model, which represent steel and aluminum, are given in Table 2.

Table 2. Material Constants for the Projectile

Component	Density (kg/m^3)	Young's Modulus (GPa)	Poisson's Ratio	Yield Stress (MPa)	Hardening Modulus (MPa)
Case	7857	207	0.3	1241	1193
End Cap	8922	207	0.3	1241	1193
Battery Housing	9459	207	0.3	1241	1193
Battery Packing	2087	69	0.33	503	69
Battery	1919	69	0.33	503	69
Data Recorder	4406	207	0.33	1241	1193
Lock Ring	9127	207	0.3	1241	1193

The cavity-expansion constants for the nose of the projectile were obtained using the method developed by Forrestal and Tzou [13] for a compressible plastic-cracked-elastic Mohr-Coulomb material with the parameters given in Table 1 and a tensile strength value of 0.1*Y*. Free surface effects described by Longcope et al. [1] and defined by the constant S_f were only applied to the nose of the projectile and the new aft-body loading effect model was applied to the shank. Radial stress on the cavity versus expansion velocity curves for the aft-body was obtained from the curves of Fig. 3 for the constant values of a/a_0 = 1.00412 and 1.010, as indicated in the small strain view of Fig. 5.

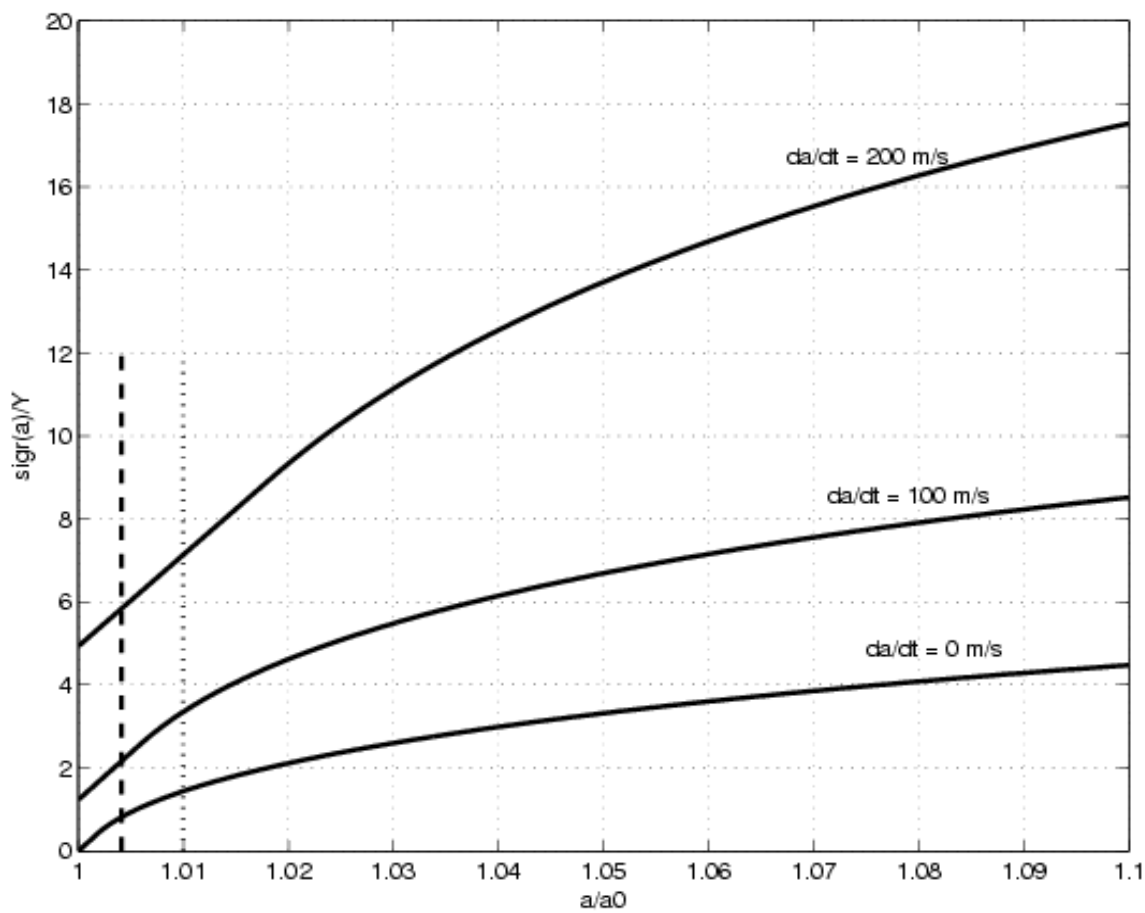

Figure 5. Detail of $\sigma_r(a)/Y$ *vs.* a/a_0 for expansion velocities between 0 and 200 m/s

A summary of the cavity expansion constants for the nose and aft-body are given in Table 3.

Table 3. Cavity Expansion Coefficients and Free Surface Effect Constants

Location	c_1 (N/m^2)	c_2 ($N\ s/m^3$)	c_3 ($N\ s^2/m^4$)	S_f
Nose	$1.06X10^8$	$4.77X10^5$	$4.5X10^3$	11.9
AFT 1.00412	$1.89X10^7$	$5.93X10^4$	$2.56X10^3$	0
AFT 1.010	$3.32X10^7$	$1.29X10^5$	$3.03X10^3$	0

In Fig.6 we compare the radial stress on the nose with the radial stress on the aft-body with $a/a_o = 1.00412$ and 1.01 over a range of expansion velocities and observe that the aft-body loading is considerably lower than that on the nose.

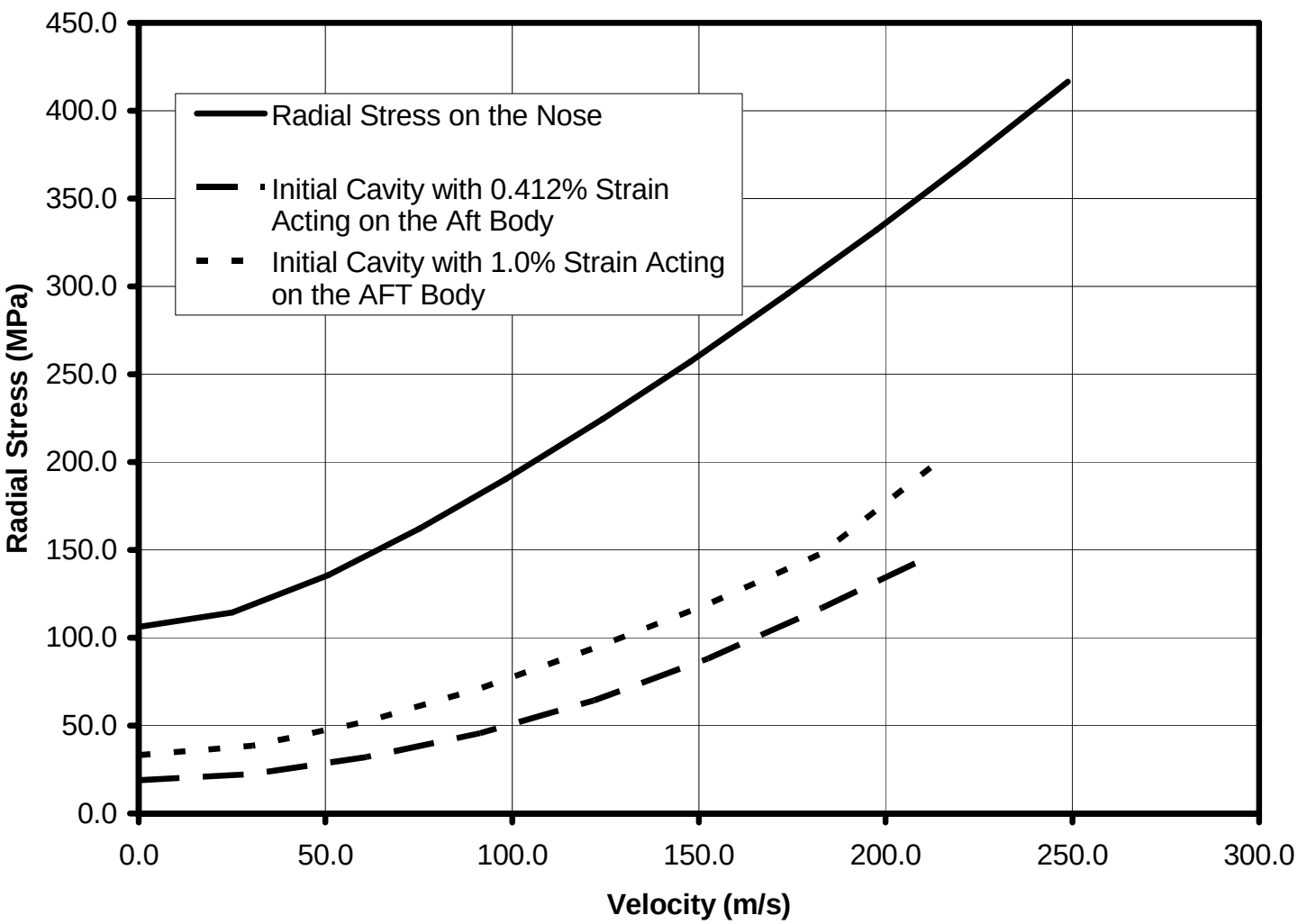

Figure 6. Radial Stress vs. Expansion Velocity for the Three Cavity Expansion Models

Results of the final projectile rest angles from the experiments and penetration simulations are compared in Table 4. The angles of attack in the plane of obliquity (R or L) were accounted for in our simulations, but those normal to it (U or D) were neglected. R and L refer to right or left, with R increasing the angle between the penetrator axis and the target normal. The simulations reasonably approximate the observed final rest angles. The error associated with $a/a_o = 1.00412$ is, in most cases, less than that when $a/a_o = 1.010$. For all the tests, the average error associated with $a/a_o = 1.00412$ is -3.05% while that associated with $a/a_o = 1.010$ is -7.29%.

Table 4. Projectile Rest Angles

Test Number	Angle of Obliquity (deg)	Velocity (m/s)	Angle of Attack (deg)	Rest Angle (deg. from normal)		
				Data	$a/a_o = 1.00412$ (% error)	$a/a_o = 1.010$ (% error)
SNL-03-12	30	286	0.3D,0.5R	50.0	43.8 (-12.0)	41.0 (-18.0)
SNL-03-15	30	334	0U,0.3R	43.0	40.9 (-4.9)	38.7 (-10.0)
SNL-03-17	30	376	0.5D,0.1L	37.2	38.4 (3.2)	36.4 (-2.2)
SNL-03-27	30	378	0.3D,0R	36.0	38.8 (7.8)	36.8 (2.2)
SNL-03-23	15	266	0.3U,0.7R	23.0	19.3 (-16.0)	18.3 (-20.0)
SNL-03-25	15	287	0.4D,0.6L	16.0	15.6 (-2.5)	15.4 (-3.8)
SNL-03-14	15	347	0.2U,0.3L	18.0	15.8 (-12.0)	15.5 (-14.0)
SNL-03-16	15	372	0.4D,0.6R	16.0	17.9 (12.0)	17.2 (7.5)

Conclusions

In this report we developed an aft-body loading model based on the expansion of a spherical cavity from an initial, finite radius. This spherical cavity-expansion model was used in conjunction with finite element simulations of penetrators striking 23MPa concrete targets at oblique angles. Comparisons of simulated penetrator rest angles with the observed rest angles showed reasonable agreement. The best correlation (with an average error of -3.05%) occurred for the aft-body loading obtained from a finite cavity having a strain of 0.412%. This aft loading is considerably less than the usual cavity expansion nose loading obtained by expanding a cavity from zero initial radius.

References

[1] D. B. Longcope, M. R. Tabbara and J. Jung, *Modeling of Oblique Penetration into Geologic Targets Using Cavity Expansion Penetrator Loading With Target Free-Surface Effects*. SAND99-1104C, Sandia National Laboratories, Albuquerque, NM, 1999.

[2] T. L. Warren, K. L. Poormon, Penetration of 6061-T6511 Aluminum Targets By Ogive-Nosed VAR 4340 Steel Projectiles at Oblique Angles: Experiments and Simulations, *Int. J. Impact Eng.*, 2001; 25: 993-1022.

[3] J. R. Koteras and A. S. Gullerud, *Presto User's Guide Version 1.05*, SAND2003-1089, Sandia National Laboratories, Albuquerque, NM, 2003.

[4] D. J. Frew and S. Gilchrist, Oblique Penetration Experiments into Low Strength Concrete Targets. Sandia National Laboratories, Albuquerque, NM 87185, USA, 2004. Private communication.

[5] R. F. Bishop, R. Hill and N. F. Mott, The Theory of Indentation and Hardness, *Proc. Roy. Soc*. 1945; 57 (3): 147-159.

[6] J. N. Goodier, On the Mechanics of Indentation and Cratering in the Solid Targets of Strain-Hardening Metal by Impact of Hard and Soft Spheres, *Proceedings of the 7th Symposium on Hypervelocity Impact III* 1965: 215-259.

[7] R. A. Hill, Theory of Earth Movement Near a Deep Underground Explosion, Memo No. 21-48, Armament Research Establishment, Fort Halstead, Kent, UK, 1948.

[8] R. A. Hill, *The Mathematical Theory of Plasticity*, London, Oxford University Press, 1950.

[9] H. G. Hopkins, Dynamic Expansion of Spherical Cavities in Metals, *Progress in Solid Mechanics*, Vol. 1, eds. I. Sneddon, and R. Hill, New York; North Holland, 1960: 85-164.

[10] M. J. Forrestal, K. Okajima and V. K. Luk, Penetration of 6061-T651 Aluminum Targets With Rigid Long Rods, *ASME Journal of Applied Mechanics*, 1988; 55: 755-760.

[11] M. J. Forrestal, K. Okajima and V. K. Luk, Penetration of Strain-hardening Targets with Rigid Spherical-nose Rods, *ASME Journal of Applied Mechanics*, 1991; 58, 7-10.

[12] M. J. Forrestal, D. Y. Tzou, E. Askari and D. B. Longcope, Penetration into Ductile Metal Targets with Rigid Spherical-Nose Rods, *Int. J. Impact Eng*., 1995; 16: 699-710.

[13] M. J. Forrestal and D. Y. Tzou, A Spherical Cavity-Expansion Penetration Model for Concrete Targets, *Int. J. Solids Structures*, 1996; 34 (31-32): 4127-4146.

[14] T. L. Warren and M. J. Forrestal, Effects of Strain Hardening and Strain-Rate Sensitivity on the Penetration of Aluminum Targets With Spherical-Nosed Rods, *Int. J. Solids Structures*, 1997; 35 (28-29): 3737-3753.

[15] M. J. Forrestal, B. S. Altman, J. D. Cargile and S. J. Hanchak, An Empirical Equation for Penetration Depth of Ogive-Nose Projectiles into Concrete Targets, *Int. J. Impact Eng.*, 1994; 15: 395-405.

[16] M. J. Forrestal and D. B. Longcope, Target Strength of Ceramic Materials for High Velocity Penetration, *J Appl. Phys*., 1990; 67: 3669-3672.

[17] T. L. Warren, S. J. Hanchak and K. L. Poormon, Penetration Of Limestone Targets By Ogive-Nosed VAR 4340 Steel Projectiles At Oblique Angles: Experiments And Simulations, *Int. J. Impact Eng.*, 2004; 30:1307-1331.

Distribution (all electronic)

Jeff Averett
US Army Corp of Engineers, ERDC
Jeff.G.Averett@erdc.usace.army.mil

Donald Cargile
US Army Corp of Engineers, ERDC
james.D.Cargile@erdc.usace.army.mil

Stephen Akers
US Army Corp of Engineers, ERDC
Stephen.A.Akers@erdc.usace.army.mil

Richard Lewis
Defense Threat Reduction Agency, ASX
richard.lewis@dtra.mil

Michael Giltrud
Defense Threat Reduction Agency, CX
mike.giltrud@dtra.mil

Philip Randles
Defense Threat Reduction Agency, CXT
philip.randles@abq.dtra.mil

Mark Green
Air Force Research Laboratory, Eglin
mark.green@eglin.af.mil

Robert Hastie
Defense Threat Reduction Agency, CXWW
robert.hastie@dtra.mil

Henry Duong, 00426
Stewart Silling, 01435
James M. Redmond, 01525
Joseph E. Bishop, 01525
Don Longcope, 01525
Joseph Jung, 01542
Aaron D. Niese, 02623
Scott McEntire, 02627
Douglas A. Dederman, 05431
James A. Dykes, 05431
John T. Foster, 05431
Eric W. Klamerus, 05431
John S. Ludwigsen, 05431
Vincent K. Luk, 05431
K. Terry Stalker, 05432
Paul Butler, 05435
Mike L. Chiesa, 08246
Technical Library, 9536

Sandia National Laboratories